The Journal of Chemical Physics

RESEARCH ARTICLE | JUNE 22 2023

Chirality induced spin selectivity: A classical spin-off

Special Collection: Chiral Induced Spin Selectivity

Yun Chen ; Oded Hod

J. Chem. Phys. 158, 244102 (2023)
https://doi.org/10.1063/5.0156491

The Journal of Chemical Physics ARTICLE scitation.org/journal/jcp

Chirality induced spin selectivity: A classical spin-off

Cite as: J. Chem. Phys. 158, 244102 (2023); doi: 10.1063/5.0156491
Submitted: 30 April 2023 • Accepted: 31 May 2023 •
Published Online: 22 June 2023

Yun Chen and Oded Hod[a)]

AFFILIATIONS

Department of Physical Chemistry, School of Chemistry, The Raymond and Beverly Sackler Faculty of Exact Sciences and The Sackler Center for Computational Molecular and Materials Science, Tel Aviv University, Tel Aviv 6997801, Israel

Note: This paper is part of the JCP Special Topic on Chiral Induced Spin Selectivity.
[a)]**Author to whom correspondence should be addressed:** odedhod@tauex.tau.ac.il

ABSTRACT

We demonstrate that angular momentum selectivity of particles traversing chiral environments is not limited to the quantum regime and can be realized in classical scenarios also. In our classical variant, the electron spin, which is central to the quantum chirality induced spin selectivity (CISS) effect, is replaced by the self-rotation of a finite-volume body. The latter is coupled to the center of mass orbital motion of the body through a helical tube via wall friction that acts as a dissipative spin–orbit coupling term. As a specific example, we study C_{60} molecules that are initially spinning in opposite senses and investigate the effect of various external control parameters on their spatial separation when driven through a rigid helical channel. We highlight resemblances and inherent differences between the quantum CISS effect and its classical variant and discuss the potential of the latter to formulate a new paradigm for enantio-separation.

INTRODUCTION

The intricate interplay between the chiral character of organic and biofunctional molecules and the electron spin degree of freedom is clearly manifested in the chirality induced spin selectivity (CISS) effect.[1–10] When an electron traverses a chiral medium, such as helically shaped molecules or molecules that possess chiral centers, its probability to transmit through the system depends on the orientation of its spin vector with respect to the direction of propagation. This effect constitutes a fundamentally important phenomenon that sheds light on the nature of the interactions between the spin of subatomic particles and their chiral molecular environment. Furthermore, it carries great potential for innovative and unprecedented technologies in the fields of spintronics[1,7,11] and enantioselectivity.[12–16]

In an effort to decipher its origin, many experiments have been designed to demonstrate and investigate the CISS effect. To that end, creative experimental approaches have been harnessed including spin-polarized photoemitted electron transmittance measurements through self-assembled monolayers of chiral molecules;[17–21] electronic transport measurements through single molecules[22] and chiral monolayers;[23–29] as well as optical,[30,31] electrochemical,[32–35] and capacitance[36–38] electron transfer measurements. Furthermore, to gain fundamental understanding of the effect, several theories have been proposed invoking spin–orbit coupling (SOC) in the chiral molecule and in the substrate and a cyclotron-like effective magnetic field that the charged electron experiences when traversing through a chiral potential.[9,39–60] Such theories indeed predict spin selectivity of transport through chiral molecules. However, to date, no single theory can fully explain the magnitude of spin-polarization measured in experiments. Recently, it has been suggested that an effective nonrelativistic SOC analog might bridge the quantitative gap between the theoretical predictions and the experimental measurements by taking into account geometric contributions to SOC.[61] Additionally, a phenomenological quantum model of the electron bath has been proposed, revealing that in the case of strong friction, the interplay between frictional dissipation and SOC makes it possible to induce a strong CISS effect even if SOC is weak.[62] Electron–phonon interactions that arise due to non-Born–Oppenheimer dynamics in the chiral environment itself have also been predicted to play a significant role in enhancing the CISS effect by naturally introducing frictional dissipation.[63–69] In particular, it was shown that the antisymmetric component of the electronic friction tensor, acting as a semiclassical Berry force, may enhance SOC and contribute to CISS.[65,69] Furthermore, it was found that energy dissipation via vibrationally assisted SOC processes may result in non-monotonic thermal behavior of the spin selectivity efficiency.[68] Therefore, major scientific efforts are being invested

striving to provide a comprehensive explanation of the mechanisms underlying the CISS effect, the origin of which is deeply rooted in the quantum nature of matter.

In light of the above, an intriguing question arises as to whether a classical variant of the CISS effect can be realized; if so, can it shed light on the nature of its quantum counterpart and does it bear any practical implication of its own? In the present study, we address these important issues by introducing such a classical variant of the CISS effect, discussing the similarities and differences it has with the quantum version, studying the dependence of classical angular momentum selectivity on various physical parameters, and pointing out potential practical implications.

RESULTS AND DISCUSSION

The classical CISS (CCISS) effect replaces the electron by a charged classical object of finite volume that crosses a helical tube serving as the chiral environment. The object rotates about an axis crossing its center of mass (COM), such that its "internal" spatial angular momentum mimics the electron spin. To realize "spin–orbit" interactions, friction is introduced at the wall of the helical tube. Unlike quantum SOC, friction represents dissipative processes that induce energy loss. Nonetheless, in the context of chirality induced selectivity, it couples the internal rotational motion of the C_{60} molecule and its center of mass trajectory within the chiral medium. Thus, in this sense, friction serves to mimic spin–orbit interactions in CCISS and not only enhance their effect as in recent quantum mechanical treatments.[63–69] When an external field is applied along the main axis of the helical tube, the propagation velocity of the object through the tube depends on the sense of rotation about its center of mass, reminiscent of the electron transmittance probability through a chiral molecule that depends on its spin state.

To demonstrate this, we present a model system consisting of a spinning C_{60} molecule that transverses a right-handed nanoscale helical tube of central helix radius of R_h = 5 nm, pitch of P_h = 7 nm, tube radius of R_{tube} = 3 nm, and total length of L = 280 nm, the central helix main axis of which is defined as the z direction (see Fig. 1). The interatomic interactions within the C_{60} molecule are modeled by the classical force-constant force-field developed by Dresselhaus and co-workers.[70,71] The conservative interactions between the atoms and the wall of the tube are represented by the Lennard-Jones (LJ) potential, whereas a dissipative frictional force is implemented near the tube wall. The C_{60} molecule is accelerated along the main axis of the helical tube by an external uniform electric field applied along the main axis of the helix. To this end, a constant electric charge is spread evenly between all its atomic centers. Further details regarding the model system and the simulation setup are provided in the Methods section.

Notably, when vertically clockwise spinning molecules encounter higher curvature surfaces of the right-handed helical tube, they are expected to experience a frictional force that promotes their forward propagation down the tube, whereas when they hit lower curvature surfaces the frictional force should oppose their forward propagation. Since the lower curvature regions are characterized by larger surface area, we expect an overall effect of deceleration of clockwise spinning molecules with respect to their non-spinning counterparts. Similarly, counterclockwise spinning molecules are expected to exhibit enhanced acceleration.

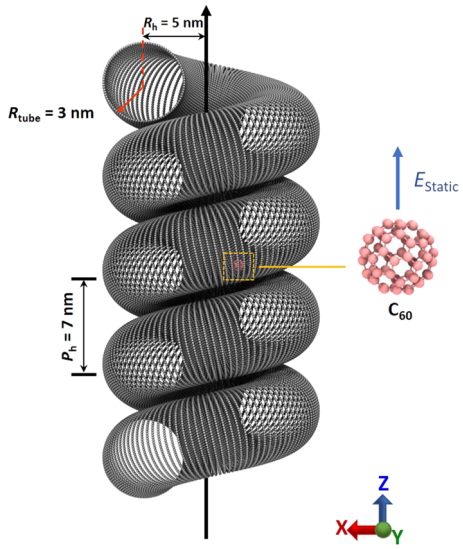

FIG. 1. Schematic illustration of the model system, consisting of a charged spinning C_{60} molecule driven through a right-handed nanoscale helical tube of central helix radius of R_h = 5 nm, pitch of P_h = 7 nm, and tube radius of R_{tube} = 3 nm via an external vertical electric field.

To show this, we start by investigating the role of the frictional forces in angular momentum selectivity. To that end, we consider a charged ($q = -1$ a.u.) C_{60} molecule spinning about the vertical axis of rotation crossing its COM with initial angular momenta of $\omega_z = 0, -0.013$, or $+0.013$ rad/fs and traversing the helical tube with wall kinetic friction coefficients of $\mu_k = 0.0, 0.1, 0.4$, or 0.8 (see the Methods section and supplementary movie 1). Since friction plays the role of SOC in our classical realization, it is expected that in its absence ($\mu_k = 0.0$), the trajectory would not depend on the initial molecular angular momentum. This is indeed the case, as can be seen in Fig. 2(a), which presents the time evolution of the vertical (z) COM coordinate of the C_{60} molecule under an external uniform static electric field of $\boldsymbol{E} = (0, 0, 0.05)$ V/Å. All three black curves trace practically the same parabolic trajectory characteristic of an accelerated object. The remaining minute differences between the three trajectories are attributed to the finite contact size between the molecule and the wall upon collision that induce slightly different impact sequences for clockwise and counterclockwise spinning buckyballs. Once friction is invoked, the trajectory becomes highly sensitive to the initial internal rotational sense of the molecule. At a friction coefficient of $\mu_k = 0.1$, counterclockwise spinning molecules (solid blue line) accelerate faster through the helical channel than their non-spinning counterparts (dotted blue line), whereas clockwise spinning molecules lag behind (dashed blue line) during the considered time frame. This results in increasing vertical spatial separation between the oppositely spinning molecules [blue line in Fig. 2(b)], thus manifesting a CCISS effect. At a higher friction coefficient of $\mu_k = 0.4$ (red lines), qualitatively similar results are obtained with a somewhat increased early time spatial separation and overall reduced acceleration due to the higher energy loss rate. When

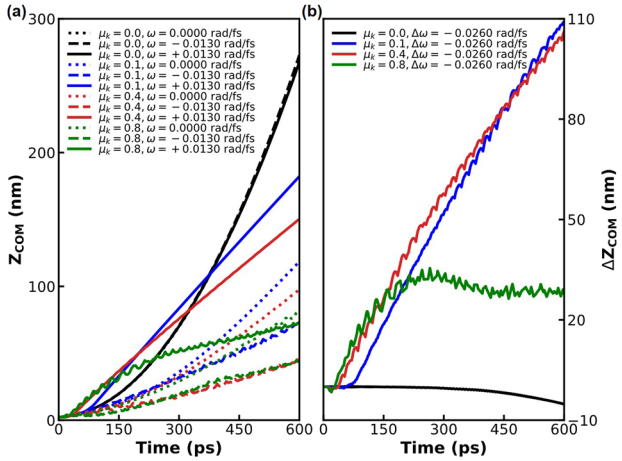

FIG. 2. Effect of kinetic friction coefficient on the trajectory of initially spinning C_{60} molecules traversing a right-handed helical tube. (a) Time evolution of the vertical COM position of counterclockwise ($\omega_z = +0.013$ rad/fs, solid lines) and clockwise ($\omega_z = -0.013$ rad/fs, dashed lines) spinning charged ($q = -1$ a.u.) C_{60} molecules, accelerated by a vertical electric field of 0.05 V/Å and experiencing kinetic friction coefficients of $\mu_k = 0.0$ (black lines), 0.1 (blue lines), 0.4 (red lines), and 0.8 (green lines) by the tube wall. Results of nonrotating molecules ($\omega_z = 0$ rad/fs) are presented for comparison by the dotted lines. (b) Time evolution of the vertical COM separation between C_{60} molecules initially spinning in opposite senses and experiencing different wall kinetic friction coefficients. Line colors match those presented in panel (a).

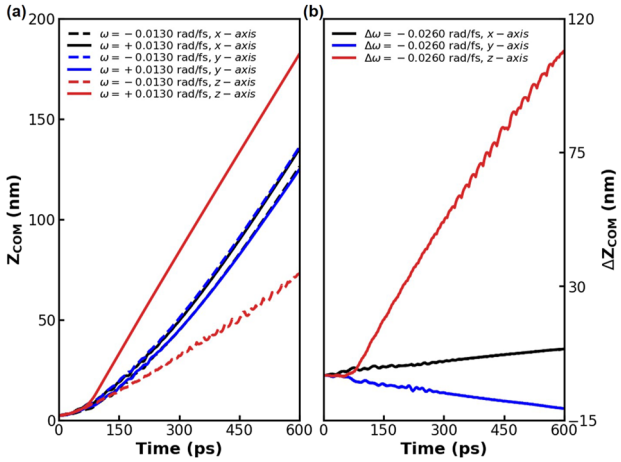

FIG. 3. Effect of initial rotational axis orientation on the trajectory of spinning C_{60} molecules traversing a right-handed helical tube. (a) Time evolution of the vertical COM position of C_{60} molecules initially spinning counterclockwise ($\omega_z = +0.013$ rad/fs, solid lines) or clockwise ($\omega_z = -0.013$ rad/fs, dashed lines) about the lateral (x—black or y—blue) or vertical (z—red) self-rotation axes. The charged ($q = -1$ a.u.) molecules are accelerated by a vertical electric field of 0.05 V/Å and experience a kinetic friction coefficient of $\mu_k = 0.1$ by the tube wall. (b) Time evolution of the vertical COM separation between C_{60} molecules spinning in opposite senses about different initial self-rotation axis orientations. Line colors match those presented in panel (a).

the kinetic friction coefficient is further increased to $\mu_k = 0.8$ (green lines), the clockwise and counterclockwise molecules rapidly reach a similar terminal velocity, resulting in saturation of their vertical distance separation. The same behavior is manifested for a left-handed helical tube, with reversed role of clockwise and counterclockwise rotating molecules (not shown).

Having established that friction induces spatial separation between oppositely spinning molecules traversing a helical tube, we now turn to evaluate the importance of the initial rotational axis orientation and the effect of angular velocity on the separation efficiency. Figure 3(a) compares the vertical COM trajectories of C_{60} molecules within the helical tube, when initially spinning in opposite senses around their lateral x (black lines) or y (blue lines) axes of rotation, to those of vertically spinning molecules (red lines). Notably, the laterally spinning molecules exhibit much smaller trajectory splitting compared to the vertically spinning counterparts. Due to symmetry considerations, the two lateral rotational axes provide the same trajectories but with reversed role of clockwise and counterclockwise spinning molecules. This is manifested in the vertical COM separation diagram [Fig. 3(b)] where, following initial transient dynamics, vertically spinning molecules exhibit a significantly larger separation than the laterally spinning ones that, in turn, have opposite sign separation curves. Naturally, the difference between the trajectories of molecules possessing initial vertical or lateral spin angular momentum depends on the details of their collision sequence with the helical tube wall. Nevertheless, our results demonstrate a general principle where the initial axis of rotation plays an important role in the spatial separation process.

Given that under the conditions considered herein, vertically spinning molecules exhibit the largest effect, we now turn to study the impact of initial vertical angular velocity on their spatial separation dynamics. Figure 4(a) compares the vertical COM trajectories of C_{60} molecules passing through the helical tube with initial angular velocities of $\omega_z = \pm 0.0065$ (black lines), ± 0.013 (blue lines), ± 0.026 (red lines), and ± 0.052 (green lines) rad/fs. Notably, clockwise spinning molecules present nearly overlapping trajectories, rapidly achieving similar terminal vertical COM velocities. Conversely, increasing the initial angular velocity of counterclockwise spinning molecules accelerates their propagation along the tube. This qualitative difference in initial angular velocity dependence exhibited by oppositely spinning molecules may be attributed to the specific initial conditions considered herein and the resulting collision sequence with surfaces of higher or lower curvature along the tube. Nevertheless, of general nature is the fact that higher initial angular velocity persists longer during the dissipative frictional motion, thus resulting in a more rapid increase in vertical spatial separation [see Fig. 4(b)].

Finally, we investigate the effect of intensity of the static electric field driving the molecules down the helical tube on the spatial separation. Figure 5(a) compares the vertical COM trajectories of C_{60} molecules passing through the helical tube under static vertical electric field intensities of $E_z = 0.01, 0.025, 0.05$ and 0.1 V/Å. Naturally, higher field intensities induce faster acceleration of the charged molecules through the tube, regardless of the initial spin sense. As a result, frictional scattering with the tube wall, and the ensuing spatial separation of oppositely spinning molecules, commences

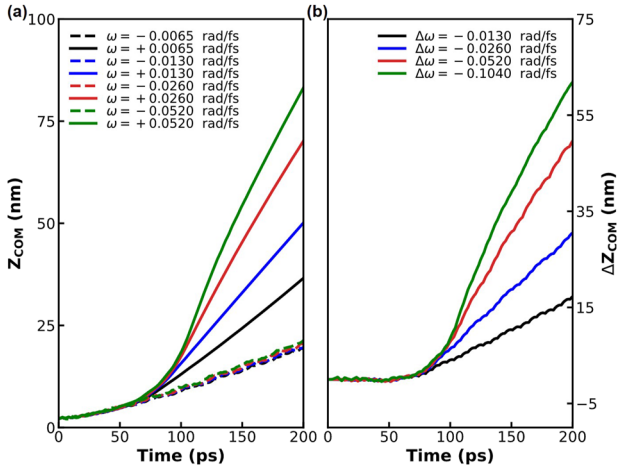

FIG. 4. Effect of initial angular velocity on the trajectory of spinning C_{60} molecules traversing a right-handed helical tube. (a) Time evolution of the vertical COM position of C_{60} molecules initially spinning with vertical velocities of $\omega_z = \pm 0.0065$ (black lines), ± 0.0130 (blue lines), ± 0.0260 (red lines), and ± 0.0520 (green lines) rad/fs, either clockwise (dashed lines) or counterclockwise (solid lines). The charged ($q = -1$ a.u.) molecules are accelerated by a vertical electric field of 0.05 V/Å and experience a kinetic friction coefficient of $\mu_k = 0.1$ by the tube wall. (b) Time evolution of the vertical COM separation between C_{60} molecules spinning in opposite senses with different initial vertical angular velocities. Line colors match those presented in panel (a).

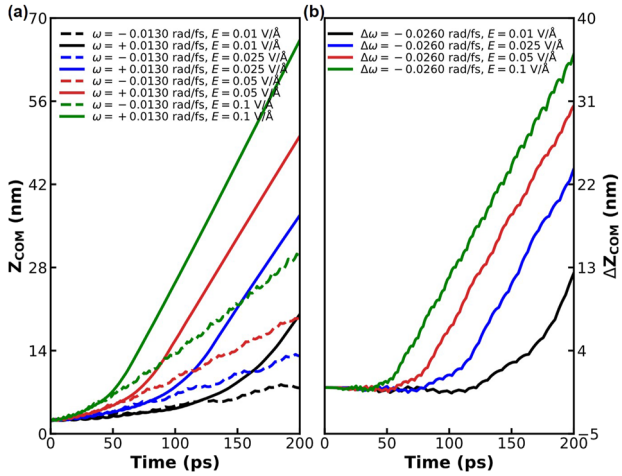

FIG. 5. Effect of vertical driving electric field intensity on the trajectory of spinning C_{60} molecules traversing a right-handed helical tube. (a) Time evolution of the vertical COM position of charged ($q = -1$ a.u.) C_{60} molecules initially spinning with a vertical velocity of $\omega_z = \pm 0.0130$ rad/fs, either clockwise (dashed lines) or counterclockwise (solid lines) under driving electric field intensities of $E_z = 0.01$ (black), 0.025 (blue), 0.05 (red), and 0.1 (green) V/Å. The molecules experience a kinetic friction coefficient of $\mu_k = 0.1$ by the tube wall. (b) Time evolution of the vertical COM separation between C_{60} molecules spinning in opposite senses under different driving electric field intensities. Line colors match those presented in panel (a).

earlier [see Fig. 5(b)]. Accordingly, terminal velocity is achieved earlier along the trajectory and is found to be weakly dependent on the field intensity for both clockwise and counterclockwise rotating molecules. This is also reflected by the long-term relative velocity between oppositely spinning molecules [depicted by the slope of the curves in Fig. 5(b)] that is practically the same for all field intensities considered.

We therefore conclude that selectivity of particles carrying angular momentum while traveling through chiral environments is not limited to the realm of quantum mechanics and can be realized also under classical conditions. In the present example, the quantum spin degree of freedom is replaced by the self-rotation of a molecule in its center of mass reference frame. The latter is coupled to the orbital motion of the molecule when driven through a helical tube via wall friction that plays the role of spin–orbit coupling. Naturally, classical angular momentum cannot truly mimic the quantized spin of particles, and dissipative friction does not faithfully imitate spin–orbit coupling. Nonetheless, the chirality induced selectivity effect variant presented herein provides a classical perspective that may help develop intuition and provide important insights regarding central factors that govern also the quantum counterpart. The classical variant may also be harnessed for molecular enantio-separation, where enantiomers of chiral molecules, manipulated by carefully designed optical sequences to rotate in opposite senses, exhibit different mobilities when crossing helical frictional channels.[74] This new frictional chiral resolution paradigm is generic in nature and may lead to efficient, low-cost, ecofriendly, and scalable enantio-separation technologies.

METHODS

The model system adopted herein consists of a C_{60} molecule traversing a rigid helical tube. The interatomic interactions of the C_{60} molecule are described by the Jishi–Mirie–Dresselhaus classical potential.[70,71] It should be noted that the correct force constants for the stretching of pentagonal and hexagonal covalent bonds are provided in Ref. 71. These are required to reproduce the normal mode frequencies presented in Table III of Ref. 70.

The helical channel is constructed around a central helix of the following parametric equation:

$$\boldsymbol{h}(\theta) = (R_h \cos(\theta), \pm R_h \sin(\theta), P_h\theta/(2\pi)), \tag{1}$$

where P_h is the helix pitch, R_h is the helix radius, θ is the polar angle of the helix, and the sign $\pm$ corresponds to the construction of a right- or left-handed helix, respectively. For simplicity, we consider helical tubes of circular cross section that lies in the plane containing the normal and binormal central helix vectors (see Fig. 6) given by

$$\boldsymbol{N}(\theta) = (-\cos(\theta), \mp \sin(\theta), 0), \tag{2}$$

and

$$\boldsymbol{B}(\theta) = \left[1 + \left(\frac{2\pi R_h}{P_h}\right)^2\right]^{-\frac{1}{2}} (\pm \sin(\theta), -\cos(\theta), \pm 2\pi R_h/P_h), \tag{3}$$

respectively. This assures that the circle normal is parallel to the tangent of the central helix given by

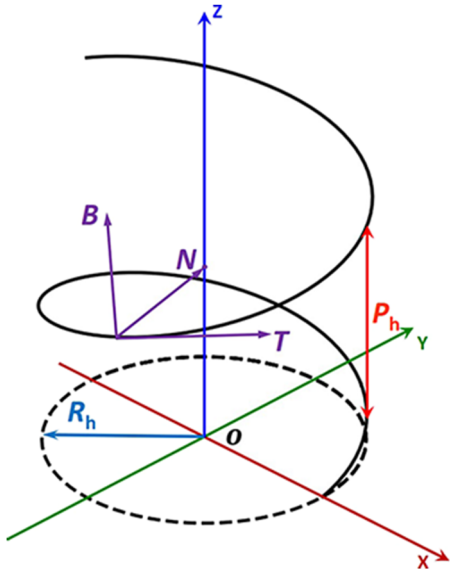

FIG. 6. Central helix of a helical tube of radius R_h and pitch P_h. ***T***, ***N***, and ***B*** are the tangent, normal, and binormal vectors of the helix, respectively.

$$\boldsymbol{T}(\theta) = \left[1 + \left(\frac{P_h}{2\pi R_h}\right)^2\right]^{-\frac{1}{2}} (-\sin(\theta), \pm\cos(\theta), P_h/(2\pi R_h)), \quad (4)$$

which makes the calculation of the interaction between the molecules and the helical tube wall easier to evaluate.

With this, the parametric representation of the helical tube is given by the following expression:

$$\boldsymbol{r}(\theta,\phi) = \boldsymbol{h}(\theta) + R_{tube}\cos(\phi)\boldsymbol{N}(\theta) + R_{tube}\sin(\phi)\boldsymbol{B}(\theta), \quad (5)$$

where ϕ is the polar angle of the tube in the **N**-**B** reference frame, and the radius of the tube has to fulfill the conditions: $R_{tube} \le R_h$ and $R_{tube} \le P_h$. For the purpose of the present study, we choose the following helical tube parameters: $R_h = 5$ nm, $P_h = 7$ nm, $R_{tube} = 3$ nm, where the main axis of the helical tube is along the z axis (see Fig. 6).

Two types of phenomenological interactions between the molecules and the wall of the rigid helical tube are considered: (i) The first is conservative forces preventing the molecules from penetrating and crossing the wall. To describe the conservative interaction of the C_{60} atoms with the helical tube wall, the LJ potential given by $V(r_\perp) = 4\varepsilon\left[(\sigma/r_\perp)^{12} - (\sigma/r_\perp)^6\right]$ acts on each atom of the molecule, where ε is the depth of the potential well, σ corresponds to the position at which the potential vanishes, and $r_\perp = R_{tube} - d_\perp$ is the shortest distance between the atom and the helical tube wall, where $d_\perp$ is the distance between the atom and the central helix, which can be calculated using an efficient numerical algorithm.[72] In our simulations, we choose LJ potential parameters fitted for graphitic systems ($\varepsilon = 2.4$ meV and $\sigma = 3.4$ Å) to represent the interaction of the C_{60} carbon atoms with the helical tube wall.[73] (ii) The second type of interactions are dissipative frictional forces, which occur whenever an atom enters the repulsive regime of the LJ potential. The kinetic friction force is modeled by the Amonton–Coulomb law,

$$\boldsymbol{F}_f = -\mu_k \boldsymbol{F}_n \hat{v}_\parallel, \quad (6)$$

where μ_k is the kinetic friction coefficient, $\boldsymbol{F}_n$ is the normal repulsive LJ force experienced by the C_{60} atom, and $\hat{v}_\parallel$ is a unit vector pointing in the direction of the atom's velocity component parallel to the helical tube wall at the point closest to it. In addition, whenever an atom resides within the repulsive interaction regime of the wall with zero parallel velocity, a similar static friction term is introduced (with $\mu_s = 0.5$), replacing the kinetic friction counterpart. Here, below the maximal value set by the static friction coefficient and the normal force, the static friction force acts in the opposite direction to the force component experienced by the atom parallel to the wall and with equal magnitude. Once the maximal static friction force is reached, kinetic friction is introduced, acting initially in the same direction.

The C_{60} molecule is initially placed with its COM located 8 Å above the lowest point of circular cross section (see Sec. 1of the supplementary material for initial position sensitivity tests) and provided with angular velocity of $\pm|\omega|$ about an axis crossing its center of mass. To drive the molecule through the helical tube, it is charged by one excess electron (modeled as 1/60 electron charge per carbon atom) and an external uniform vertical electric field is applied. The field-induced atomic force is described by $\boldsymbol{F}_E = q_i\boldsymbol{E}$, where q_i corresponds to the net charge of atom i and $\boldsymbol{E} = (0, 0, E_z)$ is the external static vertical electric field. Newton's equations of motion are propagated using the Verlet algorithm at zero initial temperature ($T = 0$ K) with a fixed time step of 0.001 fs (see Sec. 2 of the supplementary material for time-step sensitivity tests).

SUPPLEMENTARY MATERIAL

The supplementary material includes a sensitivity test with respect to the initial position of the C_{60} molecule and results of convergence tests with respect to the choice of the simulation time step.

ACKNOWLEDGMENTS

O.H. is grateful for the generous financial support of the Heineman Chair in Physical Chemistry and for partial computational support from the Tel Aviv University Center for Nanoscience and Nanotechnology.

AUTHOR DECLARATIONS

Conflict of Interest

The authors have no conflicts to disclose.

Author Contributions

Yun Chen: Data curation (equal); Formal analysis (equal); Investigation (equal); Software (equal); Validation (equal); Visualization (equal); Writing – original draft (equal); Writing – review & editing (equal). **Oded Hod**: Conceptualization (lead); Data curation (equal); Formal analysis (equal); Funding acquisition (lead); Investigation (equal); Methodology (lead); Project administration (lead); Resources (equal); Software (lead); Supervision (lead); Validation (equal); Visualization (equal); Writing – original draft (equal); Writing – review & editing (equal).

DATA AVAILABILITY

The data that support the findings of this study are available within the article and its supplementary material.

REFERENCES

[1] R. Naaman and D. H. Waldeck, Annu. Rev. Phys. Chem. **66**, 263 (2015).
[2] K. Michaeli, N. Kantor-Uriel, R. Naaman, and D. H. Waldeck, Chem. Soc. Rev. **45**, 6478 (2016).
[3] C. Fontanesi, Curr. Opin. Electrochem. **7**, 36–41 (2018).
[4] R. Naaman, Y. Paltiel, and D. H. Waldeck, Nat. Rev. Chem. **3**, 250 (2019).
[5] F. Pop, N. Zigon, and N. Avarvari, Chem. Rev. **119**, 8435 (2019).
[6] R. Naaman, Y. Paltiel, and D. H. Waldeck, J. Phys. Chem. Lett. **11**, 3660 (2020).
[7] S.-H. Yang, R. Naaman, Y. Paltiel, and S. S. P. Parkin, Nat. Rev. Phys. **3**, 328 (2021).
[8] D. H. Waldeck, R. Naaman, and Y. Paltiel, APL Mater. **9**, 040902 (2021).
[9] F. Evers, A. Aharony, N. Bar-Gill, O. Entin-Wohlman, P. Hedegård, O. Hod, P. Jelinek, G. Kamieniarz, M. Lemeshko, K. Michaeli, V. Mujica, R. Naaman, Y. Paltiel, S. Refaely-Abramson, O. Tal, J. Thijssen, M. Thoss, J. M. van Ruitenbeek, L. Venkataraman, D. H. Waldeck, B. Yan, and L. Kronik, Adv. Mater. **34**, 2106629 (2022).
[10] H. Lu, Z. V. Vardeny, and M. C. Beard, Nat. Rev. Chem. **6**, 470 (2022).
[11] Z. Shang, T. Liu, Q. Yang, S. Cui, K. Xu, Y. Zhang, J. Deng, T. Zhai, and X. Wang, Small **18**, 2203015 (2022).
[12] R. A. Rosenberg, D. Mishra, and R. Naaman, Angew. Chem. **127**, 7403 (2015).
[13] A. Kumar, E. Capua, M. K. Kesharwani, J. M. L. Martin, E. Sitbon, D. H. Waldeck, and R. Naaman, Proc. Natl. Acad. Sci. U. S. A. **114**, 2474 (2017).
[14] K. Banerjee-Ghosh, O. Ben Dor, F. Tassinari, E. Capua, S. Yochelis, A. Capua, S.-H. Yang, S. S. P. Parkin, S. Sarkar, L. Kronik, L. T. Baczewski, R. Naaman, and Y. Paltiel, Science **360**, 1331 (2018).
[15] F. Tassinari, J. Steidel, S. Paltiel, C. Fontanesi, M. Lahav, Y. Paltiel, and R. Naaman, Chem. Sci. **10**, 5246 (2019).
[16] T. S. Metzger, R. Siam, Y. Kolodny, N. Goren, N. Sukenik, S. Yochelis, R. Abu-Reziq, D. Avnir, and Y. Paltiel, J. Phys. Chem. Lett. **12**, 5469 (2021).
[17] I. Carmeli, V. Skakalova, R. Naaman, and Z. Vager, Angew. Chem., Int. Ed. **41**, 761 (2002).
[18] B. Göhler, V. Hamelbeck, T. Z. Markus, M. Kettner, G. F. Hanne, Z. Vager, R. Naaman, and H. Zacharias, Science **331**, 894 (2011).
[19] D. Mishra, T. Z. Markus, R. Naaman, M. Kettner, B. Göhler, H. Zacharias, N. Friedman, M. Sheves, and C. Fontanesi, Proc. Natl. Acad. Sci. U. S. A. **110**, 14872 (2013).
[20] M. Kettner, V. V. Maslyuk, D. Nürenberg, J. Seibel, R. Gutierrez, G. Cuniberti, K.-H. Ernst, and H. Zacharias, J. Phys. Chem. Lett. **9**, 2025 (2018).
[21] C. Wang, A.-M. Guo, Q.-F. Sun, and Y. Yan, J. Phys. Chem. Lett. **12**, 10262 (2021).
[22] A. C. Aragonès, E. Medina, M. Ferrer-Huerta, N. Gimeno, M. Teixidó, J. L. Palma, N. Tao, J. M. Ugalde, E. Giralt, I. Díez-Pérez, and V. Mujica, Small **13**, 1602519 (2017).
[23] Z. Xie, T. Z. Markus, S. R. Cohen, Z. Vager, R. Gutierrez, and R. Naaman, Nano Lett. **11**, 4652 (2011).
[24] M. Eckshtain-Levi, E. Capua, S. Refaely-Abramson, S. Sarkar, Y. Gavrilov, S. P. Mathew, Y. Paltiel, Y. Levy, L. Kronik, and R. Naaman, Nat. Commun. **7**, 10744 (2016).
[25] J. M. Abendroth, N. Nakatsuka, M. Ye, D. Kim, E. E. Fullerton, A. M. Andrews, and P. S. Weiss, ACS Nano **11**, 7516 (2017).
[26] V. Kiran, S. R. Cohen, and R. Naaman, J. Chem. Phys. **146**, 092302 (2017).
[27] S. Mishra, S. Pirbadian, A. K. Mondal, M. Y. El-Naggar, and R. Naaman, J. Am. Chem. Soc. **141**, 19198 (2019).
[28] H. Lu, C. Xiao, R. Song, T. Li, A. E. Maughan, A. Levin, R. Brunecky, J. J. Berry, D. B. Mitzi, V. Blum, and M. C. Beard, J. Am. Chem. Soc. **142**, 13030 (2020).
[29] S. Mishra, A. K. Mondal, S. Pal, T. K. Das, E. Z. B. Smolinsky, G. Siligardi, and R. Naaman, J. Phys. Chem. C **124**, 10776 (2020).
[30] B. P. Bloom, B. M. Graff, S. Ghosh, D. N. Beratan, and D. H. Waldeck, J. Am. Chem. Soc. **139**, 9038 (2017).
[31] C. Kulkarni, A. K. Mondal, T. K. Das, G. Grinbom, F. Tassinari, M. F. J. Mabesoone, E. W. Meijer, and R. Naaman, Adv. Mater. **32**, 1904965 (2020).
[32] W. Mtangi, V. Kiran, C. Fontanesi, and R. Naaman, J. Phys. Chem. Lett. **6**, 4916 (2015).
[33] W. Mtangi, F. Tassinari, K. Vankayala, A. Vargas Jentzsch, B. Adelizzi, A. R. A. Palmans, C. Fontanesi, E. W. Meijer, and R. Naaman, J. Am. Chem. Soc. **139**, 2794 (2017).
[34] K. B. Ghosh, W. Zhang, F. Tassinari, Y. Mastai, O. Lidor-Shalev, R. Naaman, P. Möllers, D. Nürenberg, H. Zacharias, J. Wei, E. Wierzbinski, and D. H. Waldeck, J. Phys. Chem. C **123**, 3024 (2019).
[35] S. Ghosh, B. P. Bloom, Y. Lu, D. Lamont, and D. H. Waldeck, J. Phys. Chem. C **124**, 22610 (2020).
[36] K. Senthil Kumar, N. Kantor-Uriel, S. P. Mathew, R. Guliamov, and R. Naaman, Phys. Chem. Chem. Phys. **15**, 18357 (2013).
[37] I. Carmeli, K. S. Kumar, O. Heifler, C. Carmeli, and R. Naaman, Angew. Chem., Int. Ed. **53**, 8953 (2014).
[38] S. Ghosh, S. Mishra, E. Avigad, B. P. Bloom, L. T. Baczewski, S. Yochelis, Y. Paltiel, R. Naaman, and D. H. Waldeck, J. Phys. Chem. Lett. **11**, 1550 (2020).
[39] E. Medina, F. López, M. A. Ratner, and V. Mujica, Europhys. Lett. **99**, 17006 (2012).
[40] M. S. Zöllner, S. Varela, E. Medina, V. Mujica, and C. Herrmann, J. Chem. Theory Comput. **16**, 2914 (2020).
[41] A. Ghazaryan, Y. Paltiel, and M. Lemeshko, J. Phys. Chem. C **124**, 11716 (2020).
[42] S. Naskar, A. Saghatchi, V. Mujica, and C. Herrmann, Isr. J. Chem. **62**, e202200053 (2022).
[43] Y. Liu, J. Xiao, J. Koo, and B. Yan, Nat. Mater. **20**, 638 (2021).
[44] S. Alwan and Y. Dubi, J. Am. Chem. Soc. **143**, 14235 (2021).
[45] Y. Wolf, Y. Liu, J. Xiao, N. Park, and B. Yan, ACS Nano **16**, 18601 (2022).
[46] Y. Adhikari, T. Liu, H. Wang, Z. Hua, H. Liu, E. Lochner, P. Schlottmann, B. Yan, J. Zhao, and P. Xiong, arXiv:2209.08117 (2022).
[47] Y. Dubi, Chem. Sci. **13**, 10878 (2022).
[48] S. Sarkar, S. Alwan, A. Sharoni, and Y. Dubi, arXiv:2211.06278 (2022).
[49] K. H. Huisman, J.-B. M.-Y. Heinisch, and J. M. Thijssen, J. Phys. Chem. C **127**, 6900 (2023).
[50] A.-M. Guo and Q.-F. Sun, Phys. Rev. Lett. **108**, 218102 (2012).
[51] N. Thanh Phuc, J. Phys. Chem. Lett. **14**, 1626 (2023).
[52] S. Naskar, V. Mujica, and C. Herrmann, J. Phys. Chem. Lett. **14**, 694 (2023).
[53] L. Wan, Y. Liu, M. J. Fuchter, and B. Yan, Nat. Photonics **17**, 193 (2023).
[54] R. Gutierrez, E. Díaz, C. Gaul, T. Brumme, F. Domínguez-Adame, and G. Cuniberti, J. Phys. Chem. C **117**, 22276 (2013).
[55] J. Gersten, K. Kaasbjerg, and A. Nitzan, J. Chem. Phys. **139**, 114111 (2013).
[56] A.-M. Guo and Q.-F. Sun, Proc. Natl. Acad. Sci. U. S. A. **111**, 11658 (2014).
[57] S. Matityahu, Y. Utsumi, A. Aharony, O. Entin-Wohlman, and C. A. Balseiro, Phys. Rev. B **93**, 075407 (2016).
[58] X. Yang, C. H. van der Wal, and B. J. van Wees, Phys. Rev. B **99**, 024418 (2019).
[59] S. Dalum and P. Hedegård, Nano Lett. **19**, 5253 (2019).
[60] M. Geyer, R. Gutierrez, and G. Cuniberti, J. Chem. Phys. **152**, 214105 (2020).
[61] A. Shitade and E. Minamitani, New J. Phys. **22**, 113023 (2020).
[62] A. G. Volosniev, H. Alpern, Y. Paltiel, O. Millo, M. Lemeshko, and A. Ghazaryan, Phys. Rev. B **104**, 024430 (2021).
[63] G.-F. Du, H.-H. Fu, and R. Wu, Phys. Rev. B **102**, 035431 (2020).
[64] J. Fransson, Phys. Rev. B **102**, 235416 (2020).
[65] X. Bian, Y. Wu, H.-H. Teh, Z. Zhou, H.-T. Chen, and J. E. Subotnik, J. Chem. Phys. **154**, 110901 (2021).
[66] J. Fransson, Nano Lett. **21**, 3026 (2021).
[67] J. Fransson, J. Phys. Chem. Lett. **13**, 808 (2022).

[68]T. K. Das, F. Tassinari, R. Naaman, and J. Fransson, J. Phys. Chem. C **126**, 3257 (2022).
[69]H.-H. Teh, W. Dou, and J. E. Subotnik, Phys. Rev. B **106**, 184302 (2022).
[70]R. A. Jishi, R. M. Mirie, and M. S. Dresselhaus, Phys. Rev. B **45**, 13685 (1992).
[71]R. A. Jishi, R. M. Mirie, M. S. Dresselhaus, G. Dresselhaus, and P. C. Eklund, Phys. Rev. B **48**, 5634 (1993).
[72]Y. Nievergelt, Nucl. Instrum. Methods Phys. Res., Sect. A **598**, 788 (2009).
[73]M. Neek-Amal, N. Abedpour, S. N. Rasuli, A. Naji, and M. R. Ejtehadi, Phys. Rev. E **82**, 051605 (2010).
[74]Y. Chen, L. Xu, M. Urbakh, and O. Hod, J. Phys. Chem. C (published online 2023).